



HAL
open science

Influence of debonding and substrate plasticity on thin film multicracking

Aurélien Doitrand, Sarah Rubeck, Sylvain Meille, Jérôme Chevalier, Philippe Steyer, Sébastien Gallois-Garreignot

► **To cite this version:**

Aurélien Doitrand, Sarah Rubeck, Sylvain Meille, Jérôme Chevalier, Philippe Steyer, et al.. Influence of debonding and substrate plasticity on thin film multicracking. *Theoretical and Applied Fracture Mechanics*, 2024, 131, pp.104375. 10.1016/J.tafmec.2024.104375 . hal-04511288

HAL Id: hal-04511288

<https://hal.science/hal-04511288>

Submitted on 19 Mar 2024

HAL is a multi-disciplinary open access archive for the deposit and dissemination of scientific research documents, whether they are published or not. The documents may come from teaching and research institutions in France or abroad, or from public or private research centers.

L'archive ouverte pluridisciplinaire **HAL**, est destinée au dépôt et à la diffusion de documents scientifiques de niveau recherche, publiés ou non, émanant des établissements d'enseignement et de recherche français ou étrangers, des laboratoires publics ou privés.



Distributed under a Creative Commons Attribution 4.0 International License

Influence of debonding and substrate plasticity on thin film multicracking

 Aurelien Doitrand¹, Sarah Rubeck^{1,2},  Sylvain Meille¹,  Jérôme Chevalier¹,
 Philippe Steyer¹, and Sébastien Gallois-Garreignot²

¹ Univ Lyon, INSA Lyon, Université Claude Bernard Lyon 1, CNRS, MATEIS, UMR5510, 69621 Villeurbanne, France, aurelien.doitrand@insa-lyon.fr

² STMicroelectronics, 850 rue Jean Monnet, Crolles, 38926, France

Multicracking of a thin brittle layer deposited on a substrate with an intermetallic layer is studied using finite fracture mechanics. Nonlinear implementation of the coupled criterion is used to predict the initiation and successive subdivisions of a periodic network of cracks considering intermetallic layer plasticity and interface debonding. Plasticity has a moderate influence on the cracking kinetics whereas debonding length has a strong influence on the saturation crack spacing. The cracking kinetics predicted numerically is more abrupt than in experiments because of the periodicity assumption, however crack spacing at saturation similar to those measured experimentally are obtained. The tensile strength and critical energy release rate of the thin brittle layer are determined by inverse identification based on the crack density variation as a function of the imposed loading. The proposed approach also enables the accurate determination of the interface critical energy release rate based on the experimentally measured debonding lengths.

Keywords thin film, multicracking, coupled criterion

1 Introduction

Multicracking in brittle thin layers deposited on a substrate may occur in multilayered assemblies depending on the stacking geometry, layer constituent stiffness contrast and loading conditions such as bending (Beuth 1992; Schulze et al. 1998; Xia et al. 2000), tensile loading (Laws et al. 1988; Ganne et al. 2002) or even thermal shock (Bahr et al. 2010; Jiang et al. 2012). It may also be induced by manufacturing residual stresses (Fu et al. 2013; Leguillon et al. 2016). Multicracking modeling was addressed based on an energy criterion requiring the knowledge of the thin layer critical energy release rate (Hashin 1985; Hashin 1996; Nairn et al. 1993; Andersons et al. 2008). These approaches were established in the framework of Finite Fracture Mechanics (FFM), which consists in considering finite crack extensions instead of infinitesimal ones as for propagation assessment in classical linear elastic fracture mechanics (LEFM). Indeed, LEFM fails assessing crack nucleation when no pre-existing cracks exist, since in these configurations the energy release rate usually tends towards zero for a vanishing crack length. FFM overcomes this drawback and allows studying crack initiation. Nevertheless, in the previously mentioned work, the authors used a single energy criterion, which revealed ineffective for some configurations (Parvizi et al. 1978; Leguillon et al. 2016). Therefore, Leguillon (2002) proposed an improvement of such approaches by considering both energy and stress criteria to predict crack initiation. The coupled criterion (CC) was applied to the modeling of cracking in functionalized thin ceramic films induced by thermal dilatation (Leguillon et al. 2014), surface cracking of an oxidized polymer under bending (Leguillon et al. 2016), multicracking in thin layers (Leguillon et al. 2017a) or ceramic surface cracking under thermal shock (Ricardo et al. 2020). In the previously mentioned studies, the CC was implemented by considering unit cells to describe the initiation and subsequent subdivisions of a periodic array of cracks. A similar approach was also applied for the modeling of crack front segmentation under mode I+III loading (Doitrand et al. 2018).

Cracking kinetics in brittle thin layers may be influenced by the presence of a metallic interlayer between the thin layer and the substrate (Macionczyk et al. 1999; Cordill et al. 2010; Taylor et al. 2013; Cordill et al. 2015). The metallic layer acts as a crack barrier preventing crack

propagation into the substrate, rather resulting in channel cracks in the thin brittle layer (Ma et al. 1998; McElhaney et al. 2004). These channel cracks may run along the entire width of the sample, as observed in ceramic layers deposited on silicon substrate (Brillet-Rouxel 2007; He et al. 2004). Cracking mechanisms and kinetics depend on both the layer thickness and stiffness contrast between the layers. For instance, it was shown that a higher stress in the substrate had to be reached in order to nucleate cracks in a thinner ceramic film (Brillet-Rouxel 2007). Moreover, Ben Cheikh et al. (2019) showed that sufficiently thin silver interlayers resulted in long continuous channel cracks whereas short cracks were observed for thicker interlayer. The change in cracking mechanism can be related to energy dissipation through metallic interlayer plasticity (Ben Cheikh et al. 2019). The previous implementations of thin layer multicracking using the CC relied on linear elastic analysis under small deformation assumption, which provides a computationally efficient implementation of the CC (Doitrand et al. 2020a). Moreover, few of these works studied the influence of a possible interface debonding ahead of the layer cracks (Leguillon et al. 2017b). Since then, the CC was extended to account for material nonlinearities (Leguillon et al. 2017b; Rosendahl et al. 2019; Doitrand et al. 2020b; Leite et al. 2021), which makes the implementation more complex compared to the linear elastic case.

The objective of this work is to study the influence of plasticity and debonding on multicracking of thin films. Thin layer multicracking experiments are described in Section 2. The multicracking model and the CC implementation considering plasticity are presented in Section 3. Finally, Section 4 focuses on the influence of substrate plasticity and debonding on cracking kinetics including a comparison between the cracking kinetics obtained numerically and experimentally.

2 Experiments

The specimens under investigation are made of three layers deposited on a thinned silicon wafer substrate (thickness: 400 μm). An ultra-low k carbon-doped silicon oxide (porous SiOC:H, 17% vol. porosity, referred to in the following as ULK) thin layer (thickness: 0.74 μm) is deposited on the substrate (Rubeck et al. 2022). An intermetallic copper layer (thickness: 2 μm) as well as a thin silicon nitride layer (thickness: 0.06 μm) are present between the silicon substrate and the ULK film. The low permittivity of the ULK enables reducing the propagation time of information in the interconnections of microelectronic chips. It thus results in improved electrical properties, which can be at the expense of their mechanical properties. Since ULK failure may compromise the electrical integrity of the integrated circuit, it is essential to characterize their fracture properties.

All the layers are successively deposited onto the silicon substrate under clean-room environmental conditions by plasma-enhanced chemical vapor deposition or electro-chemical deposition. This configuration is chosen in order to promote multicracking in the ULK layer before final failure of the specimen. The specimens, tested under four-point bending, are placed on the apparatus so that the ULK is sollicitated under tension (Figure 1a). The four-point bending

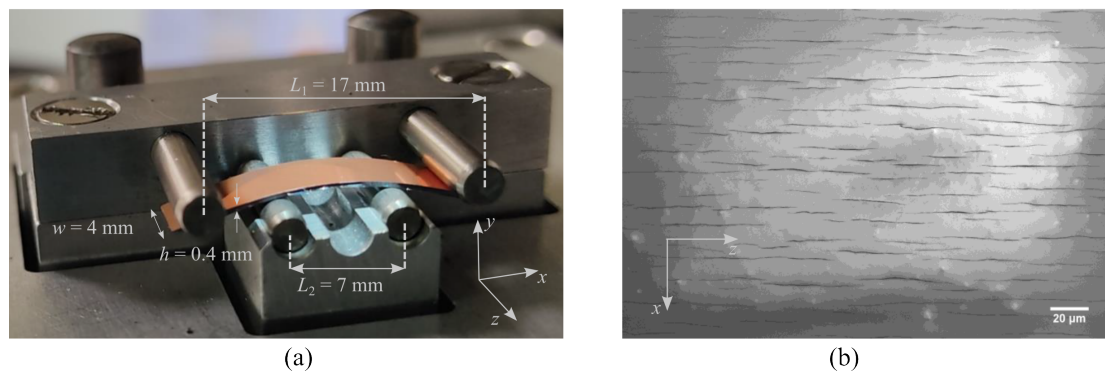


Figure 1: (a) Experimental setup for four-point bending testing of multilayer assemblies promoting (b) multicracking of the ULK layer observed by Scanning Electron Microscope (SEM) on the specimen surface.

set-up is placed in a Quattro environmental SEM (ThermoFisher, Waltham, Massachusetts, USA) chamber to perform *in situ* testing and progressive multicracking characterization. The test is stopped at different loading levels in order to make SEM observations of the face under

tension and quantify the cracking kinetics in the ULK layer (Figure 1b). At each loading level, the number of cracks, the length of each crack as well as the spacing between the cracks is quantified. Cracking occurs in the form of small disconnected cracks rather than long cracks that would span the whole specimen width. *Post mortem* optical microscope observations of the specimen also reveal the presence of debonding ahead of ULK layer cracks at the interface between the SiN layer and the copper layer (Figure 2) as noted by a change in contrast and validated by Focused Ion Beam cross section (Rubeck 2022). The typical measured debonding length lies between 2.5 and 5 microns. More details about experiments are given in (Rubeck 2022).

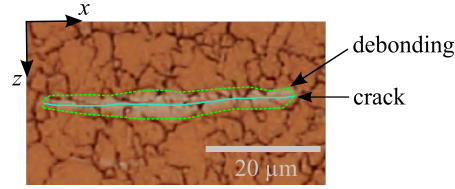


Figure 2: Optical microscope observation of the specimen top surface evidencing the presence of a crack (highlighted by plain line) and interface debonding ahead of the crack (debonding contour highlighted by dashed line).

3 Thin film multicracking modeling

Multicracking experiments may lead to a large number of cracks nucleating in a slendered layer (Figure 1b). Therefore, the finite element (FE) modeling of the successive nucleation of all these

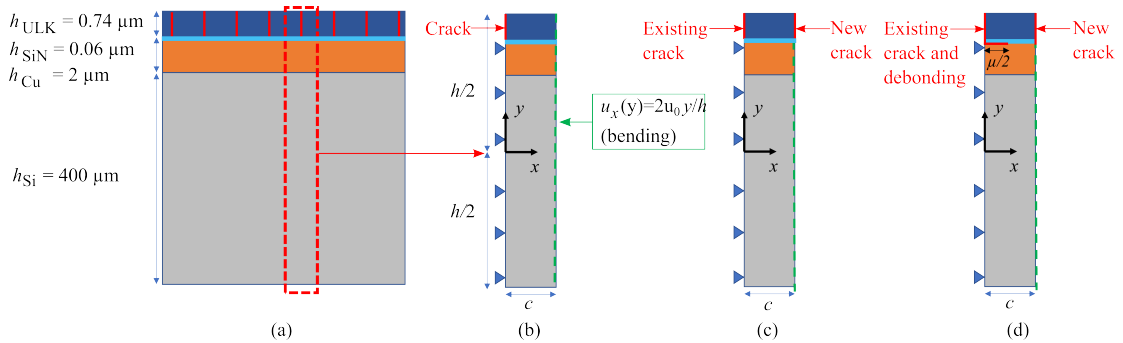


Figure 3: a) 2D side view of the specimen with the different layers from which are derived the periodic model to assess b) initiation of a first periodic crack network as well as its successive subdivisions c) without or d) with interface debonding ahead of the crack. Note the presence of the 60 nm thick SiN layer between the Cu and ULK layers, debonding occurs at the SiN/Cu interface.

cracks in the whole layer may lead to large meshes and computationally costly calculations. This problem can be solved by assuming that the crack network in the thin layer is periodic, which allows modeling only a representative unit cell (RUC) containing a central crack, that can be repeated periodically to represent the whole network of cracks (Figure 3b). Of course, this model is idealized as compared to the real crack network observed experimentally, which present repeated patterns of crack arrangement with some scattering on the crack lengths or spacings. Nevertheless, the use of a RUC enables calculating similar crack network features as in experiments such as the crack spacing or the crack density. A 2D model under small deformation assumption is adopted, which can be justified by the crack density along the specimen width being similar whatever the position along the specimen thickness at the end of the test (Figure 1b). Three RUC are used in order to model :

- the nucleation of a periodic array of cracks with a given spacing $2c$ (Figure 3b),
- the subdivision of a periodic array of cracks with a given spacing $2c$ into a periodic array of cracks with spacing c (Figure 3c),
- the nucleation and subdivision of a periodic array of cracks with a debonding (length μ ahead of the crack) (Figure 3d).

By exploiting the symmetry of the studied configuration, only half of the RUC can be represented.

Residual stresses due to the manufacturing process up to 60 MPa in the ULK layer are estimated experimentally (Rubeck 2022). They are disregarded in the present analysis and only mechanical loading is considered. The bending loading is prescribed by imposing Dirichlet boundary conditions on the edge of the RUC ($u_x(x=c) = 2u_0y/h$, where u_0 is the maximum imposed displacement magnitude). The presence of a crack is modeled by releasing the nodal Dirichlet conditions at the crack location. The RUC meshes are composed of full-integration plain strain eight-node quadratic elements, typically resulting in around 250 000 nodes in the FE model. Si, SiN and ULK layers are modeled as linear elastic materials with Young's modulus and Poisson's ratio respectively equal to $E_{\text{Si}} = 169$ GPa (Masolin et al. 2013), $E_{\text{SiN}} = 190$ GPa, $E_{\text{ULK}} = 7$ GPa (Rubeck 2022) and $\nu_{\text{Si}} = 0.33$, $\nu_{\text{SiN}} = 0.24$, $\nu_{\text{ULK}} = 0.29$. The copper layer is modeled either as linear elastic ($E_{\text{Cu}} = 135$ GPa, $\nu_{\text{Cu}} = 0.33$) or as elasto-plastic with linear hardening (yield stress σ_Y and hardening tangent modulus E_T). The influence of σ_Y and E_T on the multicracking kinetics is studied in Section 4.

3.1 The coupled criterion

The initiation and subdivision of a periodic array of cracks is modeled using the CC developed by Leguillon (2002). This criterion consists in evaluating simultaneously two conditions to guarantee the initiation of a crack. The first condition compares the tensile stress along the crack path before crack initiation to the material tensile strength σ_c . For the studied configuration of a crack initiating inside the ULK layer under a prescribed bending moment \mathcal{M}_B , it writes:

$$\sigma_{xx}(y, \mathcal{M}_B) \geq \sigma_c \quad \forall y > \frac{h}{2} - h_{\text{ULK}}. \quad (1)$$

The condition given in Equation (1) is a necessary but not sufficient condition for crack initiation. The complementary condition results from a balance of the energies before and after crack initiation:

$$\Delta W + \Delta W_k + \Delta W_p + \mathcal{G}_c \ell = \Delta W_{\text{ext}}, \quad (2)$$

where W , W_k and W_p are respectively the elastic strain, kinetic and plastic energies, W_{ext} the external force work, ℓ is the crack length and \mathcal{G}_c the critical energy release rate. Under prescribed displacements, $\Delta W_{\text{ext}} = 0$ and we assume that crack nucleation occurs simultaneously in the whole ULK layer so that $\ell = h_{\text{ULK}}$. Under quasi-static loading conditions, there is no kinetic energy prior to crack initiation, $\Delta W_k \geq 0$ therefore the energy condition can finally be rewritten as:

$$G_{\text{inc}}(\mathcal{M}_B) = -\frac{\Delta W + \Delta W_p}{h_{\text{ULK}}} \geq \mathcal{G}_c, \quad (3)$$

where G_{inc} is the incremental energy release rate. Solving the coupled criterion reverts to finding the minimum imposed bending moment \mathcal{M}_c for which both criteria are fulfilled:

$$\begin{cases} \frac{\sigma_{xx}(\frac{h}{2} - h_{\text{ULK}}, \mathcal{M}_c)}{\sigma_c} \geq 1, \\ \frac{G_{\text{inc}}(\mathcal{M}_c)}{\mathcal{G}_c} \geq 1. \end{cases} \quad (4)$$

3.2 Implementation for linear elasticity

We first present the CC implementation neglecting copper plasticity. Such an assumption simplifies the problem since it reverts to the classical CC implementation (Leguillon et al. 2017a; Doitrand et al. 2020a) under small deformation assumption and linear elastic framework. Under these conditions, the stress tensor components are proportional to the imposed bending moment and the incremental energy release rate is proportional to the square imposed bending moment \mathcal{M}_c :

$$\begin{cases} \sigma_{xx}(\mathcal{M}_e) = k\mathcal{M}_e, \\ G_{inc}(\mathcal{M}_e) = A\mathcal{M}_e^2, \end{cases} \quad (5)$$

where k and A are coefficients that can be calculated independently of the material tensile strength and critical energy release rate for a unit imposed bending moment. Then, the imposed bending moment (or equivalently maximum stress in the ULK layer σ_0) at crack initiation is determined for any $(\mathcal{G}_c, \sigma_c)$ couples as the minimum loading for which both conditions are fulfilled:

$$\mathcal{M}_c = \max\left(\frac{\sigma_c}{k}, \sqrt{\frac{\mathcal{G}_c}{A}}\right). \quad (6)$$

Therefore, solving the CC only requires the determination of k (one linear elastic calculation without crack) and A (one linear elastic calculation with a crack in the ULK layer), which is computationally efficient especially in order to establish inverse identification approaches of fracture properties.

3.3 Implementation considering plasticity

When considering plasticity in the CC implementation, Equation (5) is no longer valid because of the induced material nonlinearities. Therefore, the CC has to be solved by determining the minimum loading for which stress and energy criteria are fulfilled. It thus requires the determination of the stress and incremental energy release rate variations as a function of the applied bending moment, therefore more calculations are required compared to the linear elastic case.

Figure 4a shows the stress variation as a function of the position for an imposed bending moment so that the maximum stress in the ULK is 60 MPa for different yield stresses σ_Y and hardening tangent moduli. Because of copper plasticity, the stress is lower in the copper layer

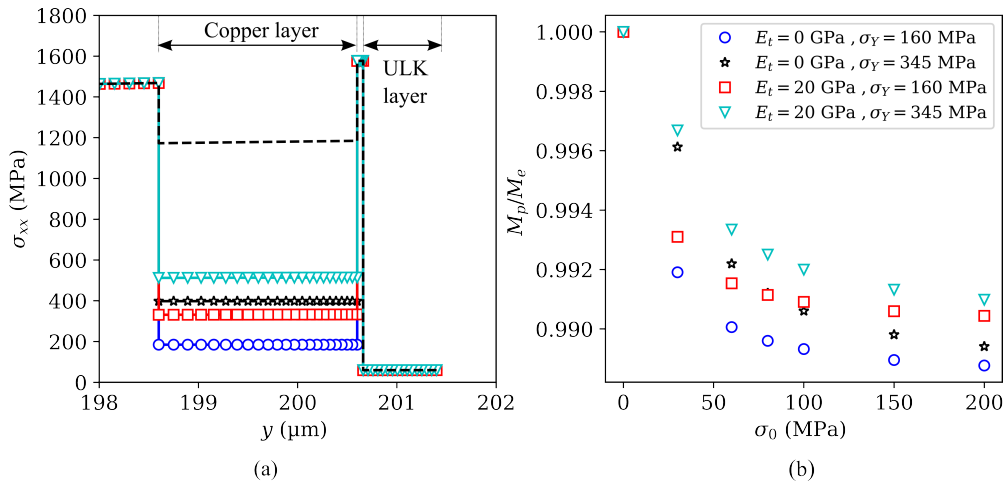


Figure 4: a) Stress variation as a function of the position in the multilayer assembly obtained for a given maximum stress in the ULK layer $\sigma_0 = 60$ MPa for different plasticity parameters (symbols) or linear elastic properties (dashed line) and b) corresponding applied bending moment as a function of the maximum stress in the ULK layer.

compared to the linear elastic case, which thus corresponds to a lower imposed bending moment. Figure 4b shows the bending moment \mathcal{M}_p that must be applied in order to reach a given maximum stress level σ_0 in the ULK layer compared to the corresponding elastic bending moment \mathcal{M}_e (Figure 4a). For a given maximum stress level σ_0 in the ULK layer, the stress in the copper layer decreases if the yield stress decreases or if the hardening tangent modulus decreases. Therefore, the bending moment that must be applied to reach a σ_0 maximum stress in the ULK layer also decreases if the yield stress decreases or if the hardening tangent modulus decreases (Figure 4b).

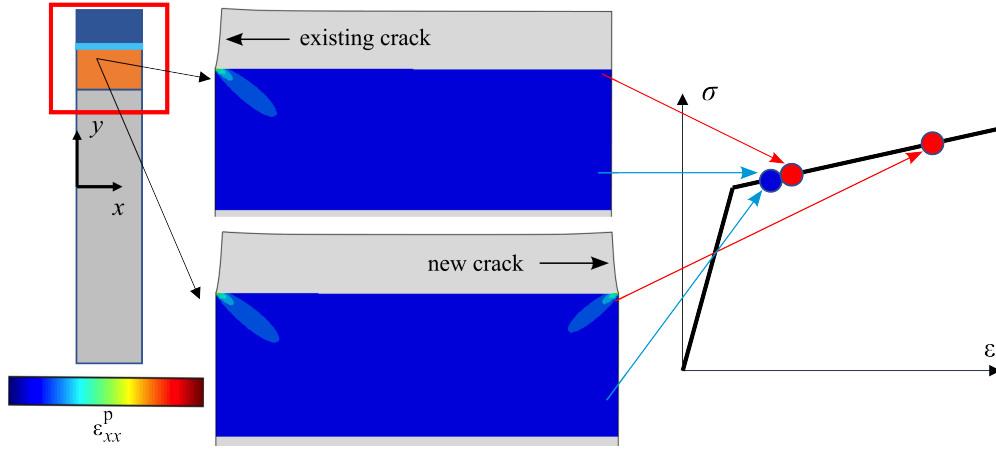


Figure 5: Plastic strain distribution in the copper layer after first crack network initiation and after crack network subdivision. Schematic representation of the stress-strain curve and local variation due to new crack initiation.

The initiation of a crack induces a stress singularity ahead of the crack tip and therefore modifies the stress and strain distribution in particular in the copper layer (Figure 5). This modification mainly occurs in the vicinity of the crack tip with a localized increase in plastic strain. Moreover, given the dimensions of the copper layer with respect to the total specimen thickness, the stress is almost homogeneous (differences smaller than 0.5%) within the copper layer before crack initiation. Therefore, it is likely that just before crack initiation, either there is no plasticity in the copper layer, or plasticity occurs in the whole copper layer (Figure 5). As a consequence, and because of the choice of a linear hardening behavior, the variation in the stress component remains linear with the bending moment. Therefore, in the particular case where the copper layer is fully plastified before crack initiation, it is still possible to exploit the proportionality of the incremental energy release rate to the square imposed bending moment. Therefore, for two bending moments \mathcal{M}_1 , \mathcal{M}_2 for which the copper layer is fully plastified :

$$G_{\text{inc}}(\mathcal{M}_2) = G_{\text{inc}}(\mathcal{M}_1) \left(\frac{\mathcal{M}_2}{\mathcal{M}_1} \right)^2. \quad (7)$$

It is highlighted in Figure 6 which shows the variation in incremental energy release rate as a function of maximum stress σ_0 in the ULK layer obtained by applying:

- i) different bending moments corresponding to maximum stresses in the ULK σ_0 in the range 10-120 MPa,
- ii) a bending moment corresponding to $\sigma_0 = 10$ MPa and using Equation (7),
- iii) a bending moment corresponding to $\sigma_0 = 120$ MPa and using Equation (7).

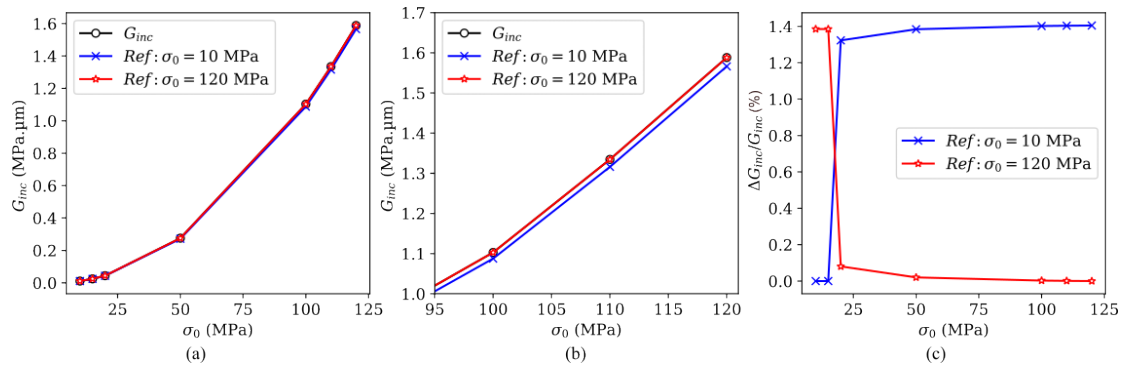


Figure 6: a-b) Incremental energy release rate as a function of the applied stress in the ULK layer obtained through direct calculation (circles) or exploiting the proportionality relation (Equation (7)) for two reference calculations and c) relative error made on G_{inc} calculation using the proportionality relation.

The applied bending moment for which plasticity starts to develop corresponds to $\sigma_0 = 20$ MPa. Therefore, for bending moments so that $\sigma_0 < 20$ MPa, no plasticity occurs in the copper layer

and Equation (7) can be used to calculate G_{inc} as in the linear elastic case. Using a reference calculation for which the applied bending moment results in $\sigma_0 > 20$ MPa and Equation (7) in order to compute G_{inc} , G_{inc} can be obtained with an error smaller than 0.2% for any other bending moments so that $\sigma_0 > 20$ MPa. Finally, in the particular case where plasticity develops in the whole copper layer before crack initiation, the proportionality between the incremental energy release rate and the square imposed bending moment can still be used, which reduces the number of calculations required for the CC application.

4 Cracking kinetics

The CC is now applied to study the initiation and subdivision of a network of cracks in the ULK layer. It requires as input the ULK tensile strength and critical energy release rate. From these quantities, a material characteristic length $\ell_{\text{mat}} = E\mathcal{G}_c/\sigma_c^2$ can be derived. From Equation (6), it can be deduced that similar variations of the stress in the ULK layer normalized by the tensile strength as a function of the inter-crack distance are obtained for a given ℓ_{mat} .

4.1 Crack network nucleation and subdivision

The CC is implemented in order to determine the cracking sequence for a given set of fracture parameters (\mathcal{G}_c, σ_c). It first consists in determining the first crack network that initiates in the ULK layer using the RUC depicted in Figure 3b. This is done by calculating the bending moment at crack initiation as a function of the crack spacing (related to the width of the RUC), or equivalently the corresponding stress in the ULK layer σ_0 . For the sake of clarity, in the sequel the results will be presented as a function of σ_0 rather than the bending moment so that it can be normalized by the ULK tensile strength. Figure 7 shows the variation of the normalized applied stress in the ULK layer as a function of the normalized crack spacing corresponding to the first crack network initiation (Figure 7a). For crack spacings sufficiently large compared to

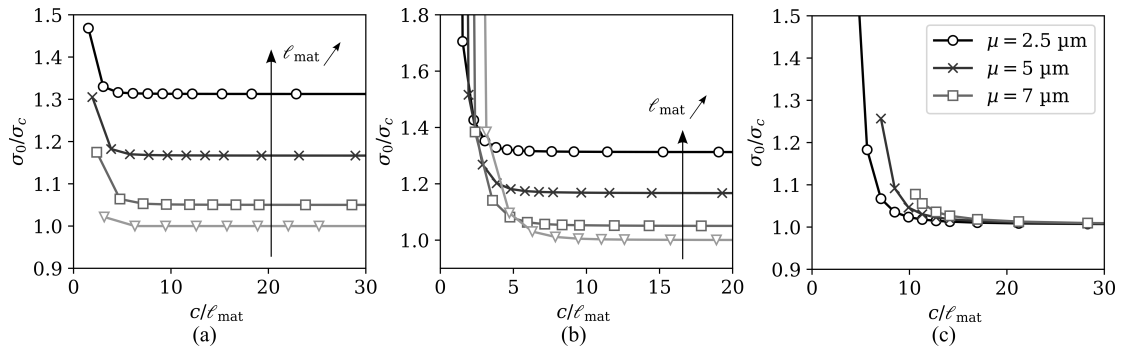


Figure 7: Normalized applied stress in the ULK layer as a function of the normalized crack spacing corresponding to a) first crack network initiation and crack network subdivision b) without or c) with debonding ahead of the ULK layer cracks.

ℓ_{mat} , the normalized applied stress in the ULK reaches a plateau which means that the cracks in the network are sufficiently far away from one another not to interact. For sufficiently small ℓ_{mat} , crack initiation is driven by the stress condition since the stress in the ULK is equal to the material tensile strength. However, for larger ℓ_{mat} , crack initiation becomes rather driven by the energy criterion and the stress in the ULK is larger than its tensile strength when crack initiation occurs. For smaller normalized crack spacings, there is an interaction between the cracks so that the loading required to initiate such a crack network increases with decreasing crack spacing. As a consequence, the minimum crack spacing at initiation can be determined as the minimum crack spacing c_{min} for which the plateau is attained.

Once the initial crack spacing is determined, the proposed model enables studying the crack network subdivision by considering the initiation of a crack at equal distance of the already nucleated cracks. It is done by applying the CC on the RUC depicted in Figure 3c and calculating the normalized applied stress as a function of the normalized crack spacing corresponding to the crack network subdivision (Figure 7b). For large enough crack spacing, the plateau is retrieved similarly as for first crack network initiation. Therefore, even if an initiation crack spacing

larger than c_{\min} is chosen, it is then possible to subdivide the crack network until a crack spacing $c_{\min}/2 \leq c < c_{\min}$ without increasing the applied loading. In the sequel, we will therefore present the results for several initial crack spacings around c_{\min} . The cracking kinetics determination finally relies on the following procedure (Leguillon et al. 2017a):

- i) Determine the initial crack spacing $c = c_0$ and the corresponding applied stress $\sigma_0(0)$,
- ii) calculate the new crack spacing $c/2$ and the corresponding imposed stress $\sigma_0(c/2)$,
- iii) repeat ii) until the crack spacing is sufficiently small so that the stress or the energy condition of the coupled criterion is not fulfilled.

An example of cracking kinetics obtained for different initial spacings in the linear elastic case without debonding is displayed in Figure 8 for further comparison with experiments. The results are given in terms of crack length per unit area (Figure 8a) and normalized crack

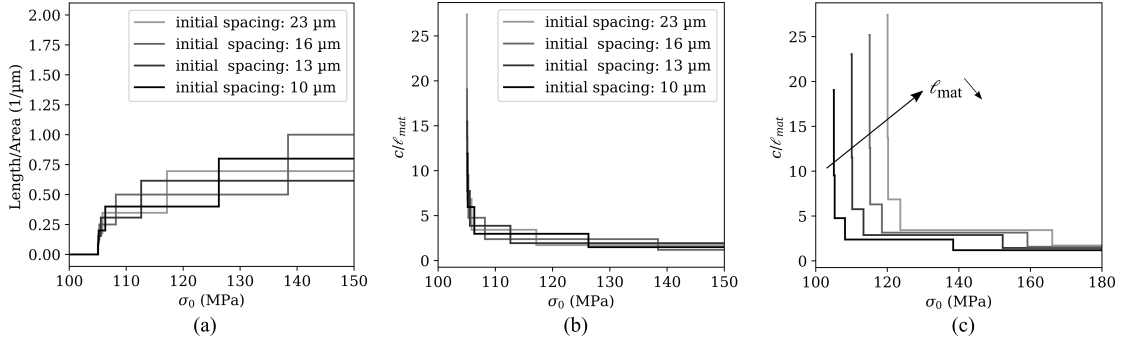


Figure 8: a) Cracking kinetics and b) crack spacing as a function of the applied stress in the ULK layer obtained using the CC for different initial crack spacings ($\ell_{\text{mat}} = 0.84 \mu\text{m}$). c) Crack spacing as a function of applied stress for different material characteristic lengths between $0.84 \mu\text{m}$ and $0.58 \mu\text{m}$ (initial crack spacing $c_0 = 16 \mu\text{m}$).

spacing (Figure 8b) variations as a function of the applied stress. The crack spacing at saturation does not depend much on the initial crack spacing, which slightly influences the variation of the crack length per unit area as a function of the applied stress since these stress values are calculated for different successive subdivisions of the crack network. The influence of ℓ_{mat} on the cracking kinetics is shown in Figure 8c for a constant \mathcal{G}_c (thus varying ℓ_{mat} by increasing σ_c) and $c_0 = 23 \mu\text{m}$ initial crack spacing. Increasing σ_c (thus decreasing ℓ_{mat}) results in increasing the applied initiation stress and delaying the successive subdivisions of the crack network, without influencing the crack spacing at saturation.

4.2 Influence of debonding

The influence of debonding on cracking kinetics is studied, first without considering plasticity of the copper layer. We recall that debonding occurs ahead of the ULK crack at the SiN/Cu interface. Figure 7c shows the normalized stress variation as a function of the normalized crack spacing considering the presence of a debonding ahead of the first crack for several debonding lengths μ . For crack spacings sufficiently large with respect to ℓ_{mat} , the plateau is also retrieved and the cracks do not interact. The crack interaction is observed for smaller crack spacings, the minimum spacing corresponding to the plateau increases with increasing debonding length. For a given crack spacing smaller than this value, the applied stress required for crack subdivision increases with increasing debonding length. The consequences on cracking kinetics are shown in Figure 9, which shows that the initial crack spacing has a moderated influence on the cracking kinetics (Figure 9a, $\mu = 2.5 \mu\text{m}$ debonding length) whereas the debonding length has a first order influence on the saturation crack spacing (Figure 9b, $c_0 = 23 \mu\text{m}$ initial crack spacing). Indeed, the larger the debonding length, the larger the saturation crack spacing and the larger the applied stress for crack network subdivision for a given spacing.

4.3 Influence of plasticity

We now focus on the influence of plasticity on cracking kinetics, first without debonding ahead of the ULK cracks. Figure 10a shows the variation of the stress in the ULK layer as a function of the normalized crack spacing corresponding to first crack network initiation and subdivision

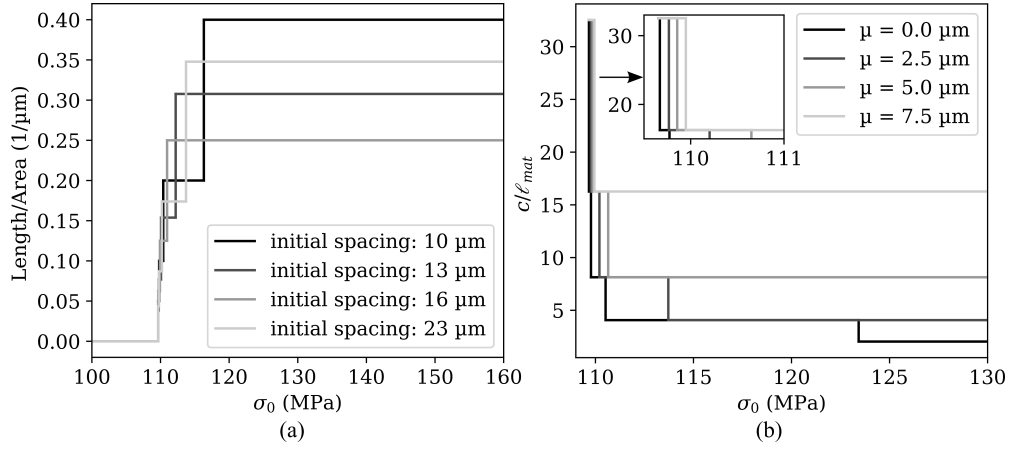


Figure 9: a) Crack length per unit area for different initial crack spacings ($\mu = 2.5$ μm debonding length) and b) normalized crack spacing for different debonding lengths ($c_0 = 23$ μm initial crack spacing) as a function of applied stress.

(initiation of a second crack network) considering either linear elastic or plastic behavior in the copper layer for a given imposed bending moment. Before first crack network initiation, the

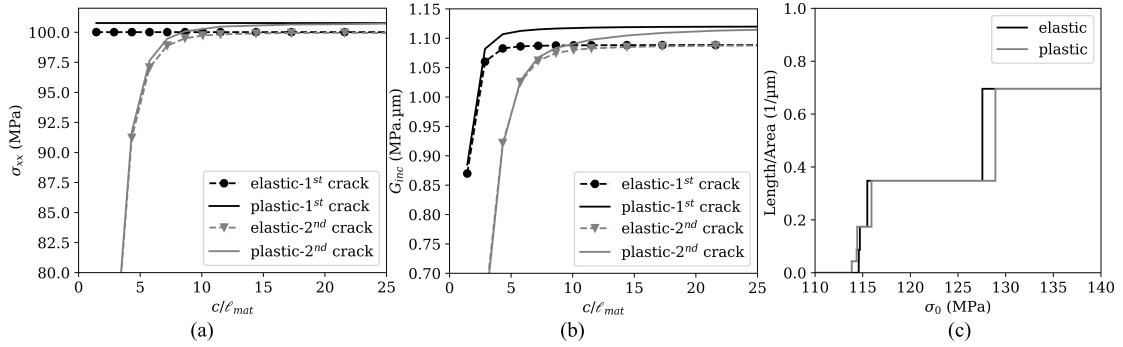


Figure 10: a) Stress in the ULK layer and b) incremental energy release rate as a function of the normalized crack spacing corresponding to either first crack network nucleation of crack network subdivision and c) crack length per unit area as a function of applied stress obtained considering or not plasticity in the copper layer.

stress in the ULK layer is constant. Its magnitude is slightly larger when considering plasticity since it results in a lower stress in the copper layer than in the linear elastic case. The incremental energy release rate for first crack network initiation is also larger for first crack network initiation considering plasticity (Figure 10b). As a consequence, plasticity in the copper layer leads to a smaller imposed bending moment at first crack network initiation. A decreasing difference in both the stress and the incremental energy release rate due to plasticity is observed with decreasing crack spacing, resulting in a slightly delayed crack network subdivision considering plasticity (Figure 10c).

Considering debonding ahead of the ULK layer crack results in a decrease in both the stress and the incremental energy release rate corresponding to crack network subdivision for sufficiently small crack spacings (Figure 11a-b). Since debonding occurs after first crack network initiation, the first crack network initiation also occurs for a smallest imposed bending moment considering plasticity, followed by a slightly delayed crack network subdivision compared to the linear elastic case (Figure 11c).

Figure 12 shows the influence on the plasticity model parameters, *i.e.* the yield stress and the hardening tangent modulus, on the cracking kinetics. Increasing the hardening tangent modulus or the yield stress results in increasing the applied bending moment at first crack initiation since the stress in the copper layer increases and therefore the stress in the ULK decreases. However, the successive crack network subdivisions are slightly delayed since for a given crack spacing, the incremental energy release rate increases with increasing hardening tangent modulus.

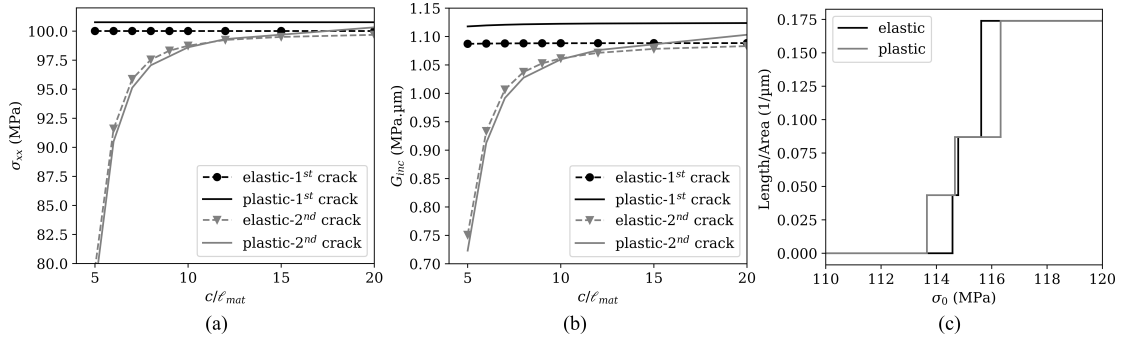


Figure 11: a) Stress in the ULK layer and b) incremental energy release rate as a function of the normalized crack spacing corresponding to either first crack network nucleation or crack network subdivision and c) crack length per unit area as a function of applied stress obtained considering or not plasticity in the copper layer in presence of $\mu = 2.5 \mu\text{m}$ interface debonding.

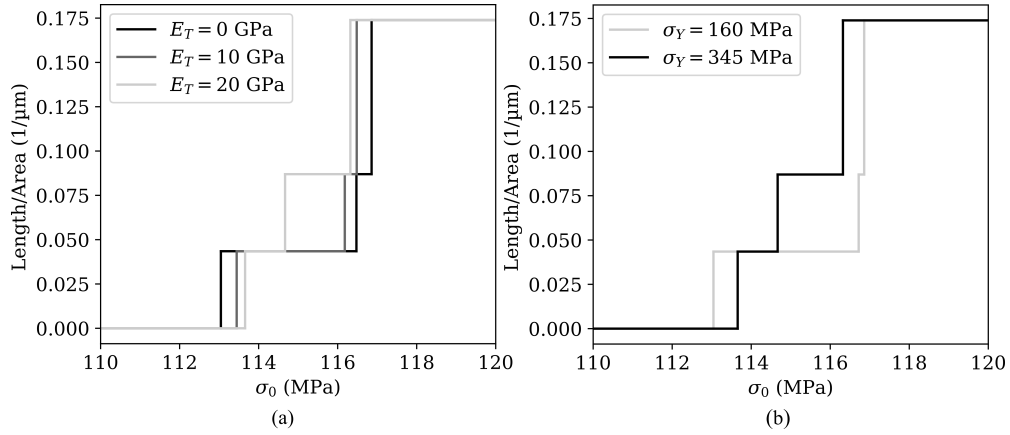


Figure 12: Crack length per unit area as a function of applied stress obtained numerically considering a $\mu = 2.5 \mu\text{m}$ debonding length a) for different hardening tangent moduli ($\sigma_Y = 345$ MPa) and b) for different yield stresses ($E_T = 20$ GPa).

4.4 Comparison with experiments

The cracking kinetics predicted with the CC considering plasticity ($E_T = 20$ GPa, $\sigma_Y = 345$ MPa) and debonding ($\mu = 2.5 \mu\text{m}$) ahead of the ULK layer cracks is now compared to the one obtained experimentally. Figure 13 shows the cracking kinetics obtained for a fixed $\mathcal{G}_c = 1.4 \text{ J/m}^2$ and $\sigma_c = 135$ MPa (Figure 13a), 142 MPa (Figure 13b) and 150 MPa (Figure 13c), therefore in a regime where the cracking kinetics is rather controlled by the ULK layer tensile strength. Figure 14

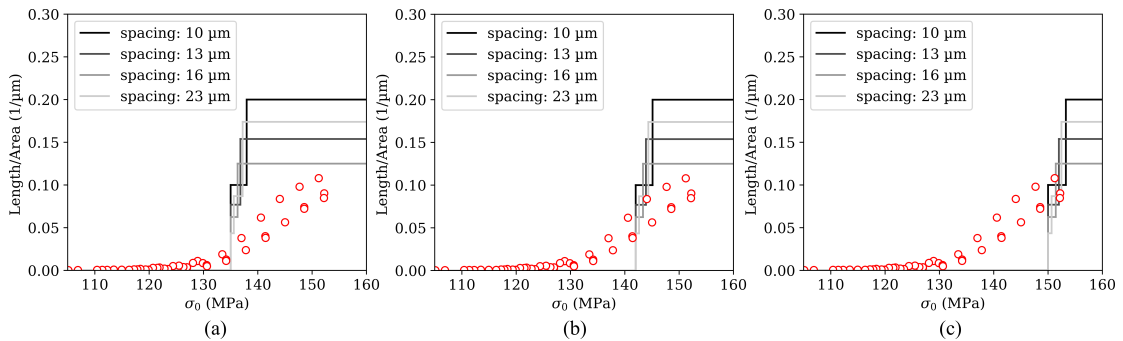


Figure 13: Crack length per unit area as a function of applied stress measured experimentally and obtained numerically for several initial spacings obtained for $\mathcal{G}_c = 1.4 \text{ J/m}^2$ and a) $\sigma_c = 135$ MPa, b) $\sigma_c = 142$ MPa and c) $\sigma_c = 150$ MPa.

shows the cracking kinetics obtained for a fixed $\sigma_c = 109$ MPa and $\mathcal{G}_c = 1.9 \text{ J/m}^2$ (Figure 14a), 2.2 J/m^2 (Figure 14b) and 2.4 J/m^2 (Figure 14c) thus corresponding to cracking kinetics controlled by the ULK critical energy release rate. The predicted cracking kinetics are more abrupt than the one measured experimentally, which is not surprising given the 2D periodic model assumption.

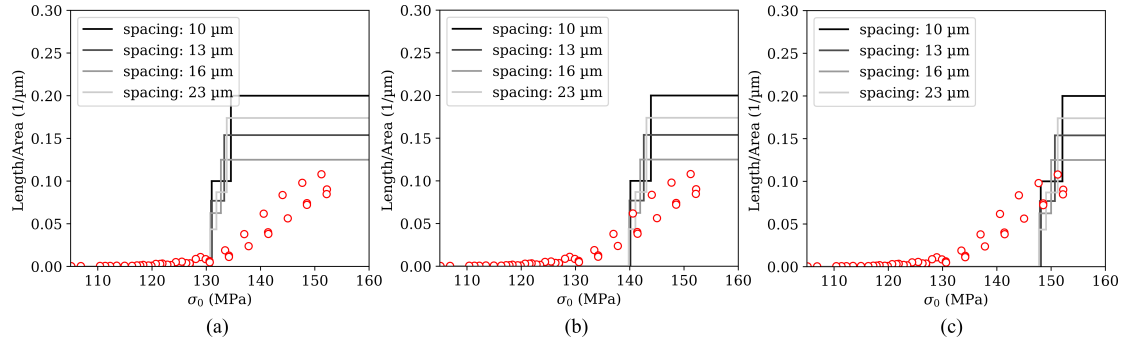


Figure 14: Crack length per unit area as a function of applied stress measured experimentally and obtained numerically for several initial spacings obtained for $\sigma_c = 109 \text{ MPa}$ and a) $\mathcal{G}_c = 1.9 \text{ J/m}^2$, b) $\mathcal{G}_c = 2.2 \text{ J/m}^2$ and c) $\mathcal{G}_c = 2.4 \text{ J/m}^2$.

Indeed, the initiation of the first crack observed experimentally is more progressive since isolated cracks initiate at different locations. Nevertheless, the periodicity assumption seems reasonable for sufficiently large crack densities. Besides, the predicted saturation crack spacing is close to the crack spacing measured experimentally at failure. Finally, the proposed approach enables estimating the fracture properties of the ULK layer through multicracking tests. The obtained critical energy release rate is in the order of magnitude of properties given in the literature.

4.5 Interface property determination

The proposed approach enables estimating the tensile strength and critical energy release rate of the ULK layer by inverse identification based on cracking kinetics obtained considering plasticity in the copper layer and debonding ahead of the ULK layer cracks. Experimentally, interface debonding lengths could only be measured based on *post mortem* optical microscope observations. Therefore, there is no available data concerning the initiation and propagation until the final debonding length. In the proposed model, the crack network subdivision was calculated assuming a constant debonding length ahead of the crack, which enables determining the cracking kinetics without assessing the possible debonding propagation. The debonding propagation may however be exploited in order to determine the critical energy release rate of the interface. Indeed, the *post mortem* observations of the specimens enable measuring debonding lengths between around 2.5 and 5 μm. It means that the initiated debonding propagated up to an arrest length. This can be traduced based on LEFM by the condition $\mathcal{G}(\mu) < \mathcal{G}_c^i$ where \mathcal{G}_c^i is the interface critical energy release rate. Figure 15 shows the variation of the energy release rate as a function of the debonding length.

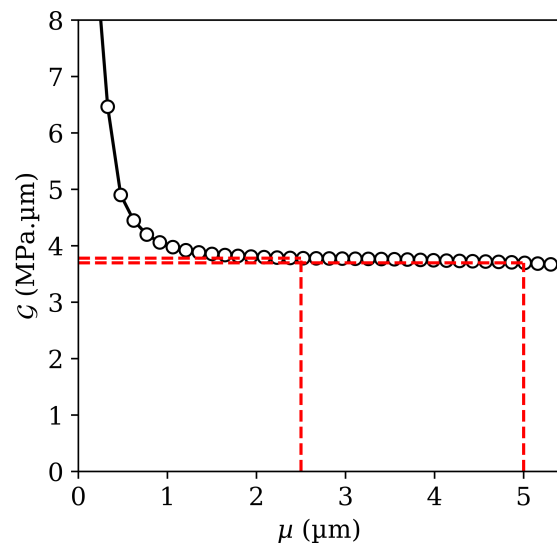


Figure 15: Energy release rate variation as a function of debonding length.

The energy release rate is a decreasing function of the debonding length, which indicates that

possible debonding ahead of the ULK layer cracks may initiate over a finite length and then propagate in a stable manner until an arrest length. The decrease in the energy release rate is relatively marked for debonding lengths smaller than $1\ \mu\text{m}$, \mathcal{G} is only slightly decreasing for larger debonding lengths. The debonding length measured experimentally lies between 2.5 and $5\ \mu\text{m}$. Therefore, it is possible to calculate the energy release rate corresponding to such debonding length, which thus provides energy release rate estimate of the interface between the silicon nitride and the copper layers. Since the energy release rate variation is moderate for debonding lengths larger than $1\ \mu\text{m}$, the identified range of interface critical energy release rate $\mathcal{G}_c^i = 3.75 \pm 0.05\ \text{J/m}^2$ is significantly less scattered. The identified interface critical energy release rate lies in the same order of magnitude as for ULK/SiC interfaces (Brillet-Rouxel et al. 2006).

5 Conclusion

Multicracking in thin brittle films deposited on a substrate with an intermetallic layer can be assessed applying the CC to the initiation and subdivision of a periodic network of cracks considering plasticity and interface debonding. Despite the induced nonlinearities, the CC implementation remains computationally efficient using a linear hardening plasticity model since the proportionality of the incremental energy release rate to the square imposed loading can still be exploited in the particular case where the whole layer is plastified. Plasticity has a relatively moderate influence on the cracking kinetics, which starts for a lower imposed bending moment and crack network subsequent subdivisions are slightly delayed compared to the linear elastic case. The saturation crack spacing mainly depends on the interface debonding length and does not depend on the initial crack spacing or the material fracture properties. The numerically predicted cracking kinetics is more abrupt than in experiments because of the periodicity assumption. However, similar crack spacing at saturation is retrieved when considering interface debonding with a length in the range of those measured experimentally despite the scattering in the measured debonding lengths. The proposed approach enables estimating a range of tensile strengths and critical energy release rates of the thin brittle layer, as well as the interface critical energy release rate with a relatively good accuracy. Future work will focus on the CC application to multicracking in 3D RUC considering plasticity and debonding in order to explain the crack arrest observed experimentally.

References

- Andersons, J., J. Modniks, Y. Leterrier, G. Tornare, P. Dumont, and J. Manson (2008). “Evaluation of toughness by finite fracture mechanics from crack onset strain of brittle coatings on polymers”. *Theoretical and Applied Fracture Mechanics* 49.2, pp. 151–157. DOI: [10.1016/j.tafmec.2007.11.002](https://doi.org/10.1016/j.tafmec.2007.11.002)
- Bahr, H., H. Weiss, U. Bahr, M. Hofmann, G. Fischer, S. Lampenscherf, and H. Balke (2010). “Scaling behavior of thermal shock crack patterns and tunneling cracks driven by cooling or drying”. *Journal of the Mechanics and Physics of Solids* 58.9, pp. 1411–1421. DOI: [10.1016/j.jmps.2010.05.005](https://doi.org/10.1016/j.jmps.2010.05.005)
- Ben Cheikh, I., G. Parry, D. Dalmas, R. Estevez, and J. Marthelot (2019). “Analysis of the multicracking mechanism of brittle thin films on elastic-plastic substrates”. *International Journal of Solids and Structures* 180-181, pp. 176–188. DOI: [10.1016/j.ijsolstr.2019.07.026](https://doi.org/10.1016/j.ijsolstr.2019.07.026)
- Beuth, J. (1992). “Cracking of thin bonded films in residual tension”. *International Journal of Solids and Structures* 29.13, pp. 1657–1675. DOI: [10.1016/0020-7683\(92\)90015-L](https://doi.org/10.1016/0020-7683(92)90015-L)
- Brillet-Rouxel, H. (2007). “Étude expérimentale et numérique des phénomènes de fissuration dans les interconnexions de la microélectronique”. Thèse de doctorat dirigée par Dupeux, Michel et Braccini, Muriel Sciences et génie des matériaux Grenoble 1 2007. PhD thesis, 1 vol. (193 p.)
- Brillet-Rouxel, H., E. Arfan, D. Leguillon, M. Dupeux, M. Braccini, and S. Orain (2006). “Crack initiation in Cu-interconnect structures”. *Microelectronic Engineering* 83.11, pp. 2297–2302. DOI: <https://doi.org/10.1016/j.mee.2006.10.053>
- Cordill, M. and A. Taylor (2010). “Flexible film systems : Current understanding and future prospects”. *JOM* 62, pp. 9–14. DOI: [10.1007/s11837-010-0096-5](https://doi.org/10.1007/s11837-010-0096-5)
- Cordill, M. and A. Taylor (2015). “Thickness effect on the fracture and delamination of titanium films”. *Thin Solid Films* 589, pp. 209–214. DOI: [10.1016/j.tsf.2015.05.021](https://doi.org/10.1016/j.tsf.2015.05.021)
- Doitrand, A. and D. Leguillon (2018). “Numerical modeling of the nucleation of facets ahead of a primary crack under mode I+III”. *International Journal of Fracture* 123(1), pp. 37–50. DOI: [10.1007/s10704-018-0305-8](https://doi.org/10.1007/s10704-018-0305-8)
- Doitrand, A., E. Martin, and D. Leguillon (2020a). “Numerical implementation of the coupled criterion: Matched asymptotic and full finite element approaches”. *Finite Element in Analysis and Design* 168, p. 103344. DOI: [10.1016/j.finel.2019.103344](https://doi.org/10.1016/j.finel.2019.103344)
- Doitrand, A. and A. Sapora (2020b). “Nonlinear implementation of Finite Fracture Mechanics: A case study on notched Brazilian disk samples”. *International Journal of Non-Linear Mechanics* 119, p. 103245. DOI: [10.1016/j.ijnonlinmec.2019.103245](https://doi.org/10.1016/j.ijnonlinmec.2019.103245)
- Fu, Y., X. Zhang, F. Xuan, S. Tu, and Z. Wang (2013). “Multiple cracking of thin films due to residual stress combined with bending stress”. *Computational Materials Science* 73, pp. 113–119. DOI: [10.1016/j.commatsci.2013.01.038](https://doi.org/10.1016/j.commatsci.2013.01.038)
- Ganne, T., J. Crépin, S. Serror, and A. Zaoui (2002). “Cracking behaviour of PVD tungsten coatings deposited on steel substrates”. *Acta Materialia* 50.16, pp. 4149–4163. DOI: [10.1016/S1359-6454\(02\)00256-2](https://doi.org/10.1016/S1359-6454(02)00256-2)
- Hashin, Z. (1985). “Analysis of cracked laminates: a variational approach”. *Mechanics of Materials* 4.2, pp. 121–136. DOI: [10.1016/0167-6636\(85\)90011-0](https://doi.org/10.1016/0167-6636(85)90011-0)
- Hashin, Z. (1996). “Finite thermoelastic fracture criterion with application to laminate cracking analysis”. *Journal of the Mechanics and Physics of Solids* 44.7, pp. 1129–1145. DOI: [10.1016/0022-5096\(95\)00080-1](https://doi.org/10.1016/0022-5096(95)00080-1)
- He, J., G. Xu, and Z. Suo (2004). “Experimental Determination of Crack Driving Forces in Integrated Structures”. *AIP Conference Proceedings* 741.1, pp. 3–14. DOI: [10.1063/1.1845831](https://doi.org/10.1063/1.1845831)
- Jiang, C., X. Wu, J. Li, F. Song, Y. Shao, X. Xu, and P. Yan (2012). “A study of the mechanism of formation and numerical simulations of crack patterns in ceramics subjected to thermal shock”. *Acta Materialia* 60.11, pp. 4540–4550. DOI: [10.1016/j.actamat.2012.05.020](https://doi.org/10.1016/j.actamat.2012.05.020)
- Laws, N. and G. Dvorak (1988). “Progressive Transverse Cracking In Composite Laminates”. *Journal of Composite Materials* 22.10, pp. 900–916. DOI: [10.1177/002199838802201001](https://doi.org/10.1177/002199838802201001)
- Leguillon, D. (2002). “Strength or toughness? A criterion for crack onset at a notch”. *European Journal of Mechanics - A/Solids* 21(1), pp. 61–72. DOI: [10.1016/S0997-7538\(01\)01184-6](https://doi.org/10.1016/S0997-7538(01)01184-6)

- Leguillon, D., O. Haddad, M. Adamowska, and P. Da Costa (2014). “Cracks Pattern Formation and Spalling in Functionalized Thin Films”. *Procedia Materials Science* 3, 20th European Conference on Fracture, pp. 104–109. DOI: [10.1016/j.mspro.2014.06.020](https://doi.org/10.1016/j.mspro.2014.06.020)
- Leguillon, D., M. Lafarie-Frenot, Y. Pannier, and E. Martin (2016). “Prediction of the surface cracking pattern of an oxidized polymer induced by residual and bending stresses”. *International Journal of Solids and Structures* 91, pp. 89–101. DOI: [10.1016/j.ijsolstr.2016.04.019](https://doi.org/10.1016/j.ijsolstr.2016.04.019)
- Leguillon, D., J. Li, and E. Martin (2017a). “Multi-cracking in brittle thin layers and coatings using a FFM model”. *European Journal of Mechanics - A/Solids* 63, pp. 14–21. DOI: [10.1016/j.euomechsol.2016.12.003](https://doi.org/10.1016/j.euomechsol.2016.12.003)
- Leguillon, D. and Z. Yosibash (2017b). “Failure initiation at V-notch tips in quasi-brittle materials”. *International Journal of Solids and Structures* 122–123, 1–13. DOI: [10.1016/j.ijsolstr.2017.05.036](https://doi.org/10.1016/j.ijsolstr.2017.05.036)
- Leite, A., V. Mantić, and F. Paris (Aug. 2021). “Crack onset in stretched open hole PMMA plates considering linear and non-linear elastic behaviours”. *Theoretical and Applied Fracture Mechanics* 114, p. 102931. DOI: [10.1016/j.tafmec.2021.102931](https://doi.org/10.1016/j.tafmec.2021.102931)
- Ma, Q., J. Xie, S. Chao, S. El-Mansy, R. Mcfadden, and H. Fujimoto (1998). “Channel Cracking Technique for Toughness Measurement of Brittle Dielectric Thin Films on Silicon Substrates”. *MRS Proceedings* 516, p. 331. DOI: [10.1557/PROC-516-331](https://doi.org/10.1557/PROC-516-331)
- Macionzyk, F. and W. Bruckner (1999). “Tensile testing of AlCu thin films on polyimide foils”. *Journal of Applied Physics* 86, pp. 4922–4929. DOI: [10.1063/1.371461](https://doi.org/10.1063/1.371461)
- Masolin, A., P. Bouchard, R. Martini, and M. Bernacki (2013). “Thermo-mechanical and fracture properties in single-crystal silicon”. *Journal of Materials Science* 48, pp. 979–988. DOI: [10.1007/s10853-012-6713-7](https://doi.org/10.1007/s10853-012-6713-7)
- McElhane, K. and Q. Ma (2004). “Investigation of moisture-assisted fracture in SiO₂ films using a channel cracking technique”. *Acta Materialia* 52.12, pp. 3621–3629. DOI: [10.1016/j.actamat.2004.04.014](https://doi.org/10.1016/j.actamat.2004.04.014)
- Nairn, J., S. HU, and J. Bark (1993). “A critical evaluation of theories for predicting microcracking in composite laminates”. *Journal of Material Science* 28, pp. 5099–5111. DOI: [10.1007/BF00361186](https://doi.org/10.1007/BF00361186)
- Parvizi, A., K. Garrett, and J. Bailey (1978). “Constrained cracking in glass fibre-reinforced epoxy cross-ply laminates”. *Journal of Material Science* 13(1), pp. 195–201. DOI: [10.1007/BF00739291](https://doi.org/10.1007/BF00739291)
- Ricardo, L., D. Leguillon, G. Parry, and A. Doitrand (2020). “Modeling the thermal shock induced cracking in ceramics”. *Journal of the European Ceramic Society* 40, pp. 1513–1521. DOI: [10.1016/j.jeurceramsoc.2019.11.071](https://doi.org/10.1016/j.jeurceramsoc.2019.11.071)
- Rosendahl, P. L., Y. Staudt, A. P. Schneider, J. Schneider, and W. Becker (2019). “Nonlinear elastic finite fracture mechanics: modeling mixed-mode crack nucleation in structural glazing silicone sealants”. *Materials and Design* 182, p. 108057. DOI: [10.1016/j.matdes.2019.108057](https://doi.org/10.1016/j.matdes.2019.108057)
- Rubeck, S. (2022). “Investigation of aging and cracking mechanisms in advanced ceramic materials for microelectronics. Micro and nanotechnologies/Microelectronics. Université de Lyon, 2022”. DOI: <https://theses.hal.science/tel-03860220>
- Rubeck, S., V. Cartailier, V. Coutellier, G. Imbert, S. Gallois-Garreignot, S. Meille, P. Steyer, and J. Chevalier (2022). “Effect of accelerated hydrothermal aging on the durability of Si-based dielectric thin films”. *Microelectronic Engineering* 264, p. 111858. DOI: <https://doi.org/10.1016/j.mee.2022.111858>
- Schulze, G. and F. Erdogan (1998). “Periodic cracking of elastic coatings”. *International Journal of Solids and Structures* 35.28, pp. 3615–3634. DOI: [10.1016/S0020-7683\(97\)00228-X](https://doi.org/10.1016/S0020-7683(97)00228-X)
- Taylor, A., M. Cordill, L. Bowles, J. Schalko, and G. Dehm (2013). “An elevated temperature study of a Ti adhesion layer on polyimide”. *Thin Solid Films* 531, pp. 354–361. DOI: [10.1016/j.tsf.2013.01.016](https://doi.org/10.1016/j.tsf.2013.01.016)
- Xia, Z. and J. Hutchinson (2000). “Crack patterns in thin films”. *Journal of the Mechanics and Physics of Solids* 48.6, pp. 1107–1131. DOI: [10.1016/S0022-5096\(99\)00081-2](https://doi.org/10.1016/S0022-5096(99)00081-2)

Authors' contributions Aurélien Doitrand performed numerical simulations and drafted the manuscript. Sarah Rubeck carried out the experiments. All authors developed the methodology, conceived of the study, and participated in its design, coordination, and critical review of the manuscript. All authors read and approved the final manuscript.

Ethics approval and consent to participate Not applicable.

Consent for publication Not applicable.

Competing interests The authors declare that they have no competing interests.

Open Access This article is licensed under a Creative Commons Attribution 4.0 International License, which permits use, sharing, adaptation, distribution and reproduction in any medium or format, as long as you give appropriate credit to the original author(s) and the source, provide a link to the Creative Commons license, and indicate if changes were made. The images or other third party material in this article are included in the article's Creative Commons license, unless indicated otherwise in a credit line to the material. If material is not included in the article's Creative Commons license and your intended use is not permitted by statutory regulation or exceeds the permitted use, you will need to obtain permission directly from the copyright holder. To view a full copy of this license, visit <http://creativecommons.org/licenses/by/4.0/>.